EFDA–JET–PR(10)58

G.P. Maddison, C. Giroud, G.K. McCormick, B. Alper, G. Arnoux, M.N.A. Beurskens, P.C. da Silva Aresta Belo , A. Boboc, A. Brett, S. Brezinsek, I. Coffey, S. Devaux, P. Devynck, T. Eich, R. Felton, W. Fundamenski, J. Harling, A. Huber, S. Jachmich, E. Joffrin, P.J. Lomas, P. Monier-Garbet, P.D. Morgan, M.F. Stamp, G. Telesca H. Thomsen, I. Voitsekhovitch and JET EFDA contributors

Demonstration of Real-Time Control of Impurity Seeding Plus Outboard Strike-Point Sweeping in JET ELMy H-mode Plasmas

Demonstration of Real-Time Control of Impurity Seeding Plus Outboard Strike-Point Sweeping in JET ELMy H-mode Plasmas

G.P. Maddison [1], C. Giroud [1], G.K. McCormick [2], B. Alper [1], G. Arnoux [1], P.C. da Silva Aresta Belo [3], M.N.A. Beurskens [1], A. Boboc [1], A. Brett [1], S. Brezinsek [4], I. Coffey [5], S. Devaux [2], P. Devynck [6], T. Eich [2], R. Felton [1], W. Fundamenski [1], J. Harling [1], A. Huber [4], S. Jachmich [7], E. Joffrin [8], P.J. Lomas [1], P. Monier-Garbet [6], P.D. Morgan [1], M.F. Stamp [1], G. Telesca [7], H. Thomsen [2], I. Voitsekhovitch [1] and JET EFDA contributors*

JET-EFDA, Culham Science Centre, OX14 3DB, Abingdon, UK

[1]EURATOM-CCFE Fusion Association, Culham Science Centre, OX14 3DB, Abingdon, OXON, UK
[2] Max-Planck IPP, EURATOM Association, D-85748 Garching, Germany
[3] IPFN, EURATOM-IST Associação, 1096 Lisbon, Portugal
[4]IEF Plasmaphysik Forschungszentrum Jülich, Association EURATOM-FZ Jülich, Germany
[5] Queen's University Belfast, University Road, Belfast BT7 1NN, Northern Ireland, UK
[6] CEA, IRFM, F-13108 St Paul lez Durance, France
[7] Association 'Euratom-Belgian state', Ecole Royale Militaire, B-1000 Brussels, Belgium
[8] EFDA-JET CSU, Culham Science Centre, OX14 3DB, Abingdon, OXON, UK
** See annex of F. Romanelli et al, "Overview of JET Results", (23rd IAEA Fusion Energy Conference, Daejon, Republic of Korea (2010)).*

Preprint of Paper to be submitted for publication in
Nuclear Fusion Letters

ABSTRACT

Strike-point sweeping and Real-Time-Controlled (RTC) impurity seeding are both expected to be needed on JET following its upgrade to an all metal wall with enhanced neutral-beam heating. First trials have combined these techniques in high-triangularity Type I H-mode plasmas, using a VUV spectroscopic signal for feedback control of nitrogen injection. Compared with earlier unswept feedforward counterparts, similar strong mitigation of divertor heat load between ELMs was achieved in swept RTC cases for less than half the integrated nitrogen input and correspondingly less adverse effect upon other properties. Both sweeping and RT control contributed to this improvement. Time-average normalised energy confinement $\langle H_{95y} \rangle_t \sim 1$, Greenwald density fraction $\langle f_{Gwd} \rangle_t \sim 0.9$, and particularly purity denoted by effective ionic charge $\langle Z_{eff} \rangle_t \approx 1.7$, all remained closer to good reference levels. Transient effluxes in ELMs were also less affected, however, and would require separate active control.

INTRODUCTION

In a major next upgrade of the JET tokamak (major radius 3m, minor radius ≈ 1m), its plasma-facing components are all being replaced with metal surfaces [1,2], primarily to pursue lower long-term retention of fuel species than has commonly been observed in carbon machines [3,4,5]. Its main torus will be lined with beryllium, while the divertor will be refurbished with tungsten-coated CFC side and base walls [2], plus a solid tungsten main load-bearing plate designed to receive the Outboard Strike-Point (OSP) and Scrape-Off Layer (SOL) [6]. These new ITER-Like Wall (ILW) materials imply revised operational constraints on power loads and adjacent plasma temperatures [7], necessitating adaptation of ITER-relevant scenarios under development on JET. One key element arises from radial segmentation of the bulk tungsten plate into four toroidal stacks (see Fig.1(a)), within the constituent lamellae [6] of each of which thermal conductivity will be extremely high, but between which it will be very low. In order to make best use of the energy-handling capacity of the whole plate (≈ 50MJ per stack for a wetted fraction of ≈ 0.7) [7], it is anticipated discharges will therefore routinely adopt cyclic sweeping of the OSP, to ensure the SOL contacts most of its area. In addition, moderation of near-target plasma temperatures, together with intended reduction of the hitherto large fraction of carbon radiation in JET, suggest raising recycling with enhanced fuelling and maintaining radiation by seeding with extrinsic impurities. These strategies will particularly become essential as additional heating is progressively increased up to ≈ 34MW for ≤ 20s in a simultaneous upgrade of the Neutral-Beam Injection (NBI) system [8]. Initial experiments on feedforward fuelling and seeding have been carried out [9,10], but it is expected that more robust and stationary conditions in longer pulses will require Real-Time Control (RTC) of the seeding process (e.g. as found previously in limiter plasmas on the TEXTOR [11,12], and divertor plasmas on the ASDEX Upgrade [13,14], devices). In this note, we report preliminary tests of feedback-controlled nitrogen seeding of ELMy H-mode states on JET, combined with wide sweeping of the OSP.

Attention has been focused upon Type I ELMy H-mode conditions in a high-triangularity

($^{av} \approx 0.41$) single-null-divertor configuration at field and current 2.7 T, 2.5 MA, with NBI additional heating of 13-15MW. A further 1-2.5MW of ion-cyclotron-resonance-frequency waves were also injected to promote regular sawteeth [15], while edge safety factor was raised slightly to $q_{95} \approx 3.5$ to help avoid Neo-classical Tearing Modes (NTMs). Strong magnetic shaping was deliberately chosen in order to access the JET domain where fuelling can be increased without degrading the edge pedestal and global energy confinement [16,17]. Triangular-waveform sweeping of the OSP at 4Hz was then introduced, with a radial amplitude of ≈ 10cm, which as indicated by the EFIT equilibria in Fig.1(a) would be wide enough in the ILW for the SOL to touch three of its four bulk-W toroidal stacks. The time series of such magnetic reconstructions is verified in Fig.1(b) against the actual OSP position measured by fast infra-red thermography [18], framing in all experiments here at ≈ 12kHz. Most plasma properties were little affected by OSP sweeping, with e.g. diamagnetic stored energy and central line-average electron density from far-infra-red interferometry fluctuating by at most a few percent, within the range accompanying ELM perturbations in unswept reference pulses. However, recycling oscillated conspicuously in synchrony with sweeps, as revealed by the visible spectroscopic (D) trace superimposed in Fig.1(b). Recycling was highest when the OSP was farthest from the pump, and lowest when the OSP was closest to it, with total radiated power tending to follow the same variation too, by ≈ ±20%, at least between ELMs. Furthermore, ELMs were themselves clearly influenced by sweeping, from Fig.1(b) evidently being more likely when correlated recycling was higher, and less likely vice versa. This may partly have depended upon corresponding changes of ≈ ±6% - ≈ ±10% in lower and upper triangularity, but detailed time-dependent modelling would be required properly to resolve such interplay of plasma properties, sources and stability.

Previous feedforward experiments had identified a level of deuterium puffing itself sufficient to yield substantial moderation of divertor heat loads between ELMs [9,10], and this same waveform with time-average level of $\langle \Phi_D \rangle_t \approx 2.8 \times 10^{22}$ electrons/s was kept throughout the RTC trials, i.e. seeding was meant to extend, and potentially to be accentuated by [13], this elevated recycling effect. Nitrogen was chosen as the seed species owing to its beneficial impact upon inter-ELM and even ELM effluxes found before [9,10], and because of its positive effect upon confinement observed in the all-W ASDEX Upgrade machine [14]. Using nitrogen input into the outboard side of the divertor as actuator (see Fig.1(a)), the most obvious RT sensor signal would be a bolometric one conveying radiated power, but earlier feedforward cases had already disclosed that the two quantities are not generally linearly related [9,10] ; consequently an initial test of total radiated power as sensor failed stably to match set demand levels. Alternatively, a spectroscopic sensor should be more directly related to actual nitrogen abundance for roughly constant photon efficiency, including any shot-to-shot legacy (i.e. incomplete removal in between), which is appreciable in the carbon machine [9,10]. Their explicit connection should also support applicability of the technique in the ILW where nitrogen recycling and retention are likely to be different. A Vacuum Ultra-Violet (VUV) nitrogen line at 20.93nm (denoted NVA) was therefore chosen for the RT sensor, viewing the inboard side of the

divertor so that movement during SP sweeping always remained within the spectrometer sight-line (see Fig.1(a)). Owing to a significant latency of ≈ 0.5s in the physical gas response to changes in its request, a phase-lead compensator [19] was found to be the most stable design of RT controller, based on a cycle time of 10 ms [20]. First-order filters with respective time constants of 0.05s, 0.1s were added to remove ELMs from the input and to avoid excessive piezovalve switching by the output. Just two open-loop pulses were then sufficient to calibrate the network, yielding a controller transfer function $5(s + 1) / (s + 5)$ in the usual Laplace domain. An effective scan of NVA demand level in the following RTC series is shown in Fig.2, where the almost perfectly linear response of (non-RT) NVA radiance, averaged over intervals 50% - 90% of the way between consecutive ELM peaks [9,10] in a 2s flat-top window, is apparent. Insets illustrate the RT network action in two sample shots, with a certain fractional offset ($\langle \mathrm{NVA} \rangle_t^{\mathrm{sensor}} / \mathrm{NVA}^{\mathrm{demand}} \approx 0.6$-$0.7$) implying the gain had not been fully optimised.

Results for the RTC nitrogen-seeding scan are summarised in Figs.3 & 4 . Quantities in each shot are time-averaged in a steady 2s flat-top window, either over 50% - 90% segments of the periods between ELMs (abscissa in both figures, ordinates in Fig.3), to avoid each post-ELM-crash recovery phase [9,10], or for more slowly sampled items just over the whole 2s window including ELMs (ordinates in Fig.4). "Error bars" for each point are then actually the square root of variance in time, but evaluated separately above and below the mean to allow for asymmetric distributions. Points are also marked to show those plasmas incurring (4,3) NTMs (cross symbols), which may have adversely affected their performance. Remaining cases were either free of modes, or occasionally involved only milder, higher-order NTMs, which are ignored. Plotting data as functions of inter-ELM-averaged NVA radiance $\langle \mathrm{NVA} \rangle_t^{\mathrm{i\text{-}E}}$ immediately takes account of any shot-to-shot legacy, its extent being clearly revealed by those pulses with no direct seeding (labelled "0"). Reference cases are recalled from the preceding unswept feedforward series at lowest fuelling and the selected level of $\approx 2.8 \times 10^{22}$ electrons/s, for comparison purposes. The subsequent series including RTC experiments is then discriminated by bold outlining, and commenced with a plain unswept unseeded repeat at low fuelling (blue outlined circle) to confirm reasonable reproducibility. Following pulses with first OSP sweeping then adding RTC nitrogen seeding are depicted by outlined diamonds. For clarity, the combined techniques examined are reiterated in Table 1 .

Like most properties, total radiation fraction between ELMs $\langle f_{\mathrm{rad}}^{\mathrm{tot}} \rangle_t^{\mathrm{i\text{-}E}}$ (top left pane Fig.3) tended to remain more constant within error bars throughout the swept RTC series. Thus it was somewhat lower for least and highest $\langle \mathrm{NVA} \rangle_t^{\mathrm{i\text{-}E}}$ than in the unwept feedforward counterparts, which as mentioned above exhibited a markedly non-monotonic variation. Conversely, the estimated ratio of emission from the divertor and X-point vicinity to that from the bulk region above it, $\langle f_{\mathrm{rad}}^{\mathrm{div}} \rangle_t^{\mathrm{i\text{-}E}} / \langle f_{\mathrm{rad}}^{\mathrm{bulk}} \rangle_t^{\mathrm{i\text{-}E}}$ (bottom left pane Fig.3), reached a larger value even in the initial unseeded unswept case at higher fuelling (outlined orange circle). This did still incorporate one additional change from the feedforward plasmas, namely the start-up was adjusted to place the OSP earlier on the main load-bearing tile, thereby minimising power which will land on neighbouring W-coated base tiles in the ILW. The

impact on $\langle f_{\mathrm{rad}}^{\mathrm{div}} \rangle_{\mathrm{t}}^{\mathrm{i\text{-}E}} / \langle f_{\mathrm{rad}}^{\mathrm{bulk}} \rangle_{\mathrm{t}}^{\mathrm{i\text{-}E}}$ apparently produced may have been due to poorer conditioning of / divertor retention from these side surfaces, but anyway gradually disappeared for increasing $\langle \mathrm{NVA} \rangle_{\mathrm{t}}^{\mathrm{i\text{-}E}}$ until RTC and feedforward instances realised approximately the same balance of divertor to bulk radiation for highest nitrogen radiance.

Accompanying thermographic data on average power landing on the whole outboard target between ELMs, normalised by total input power, $\langle P_{\mathrm{outb.\ tgt}} \rangle_{\mathrm{t}}^{\mathrm{i\text{-}E}} / \langle P_{\mathrm{in}} \rangle_{\mathrm{t}}$ (bottom right pane Fig.3), demonstrate that mitigation of inter-ELM heat load was indeed as pronounced with swept RTC seeding as in matching unswept feedforward pulses. While both approaches reached very low power fractions, though, the insets for respective cases at highest $\langle \mathrm{NVA} \rangle_{\mathrm{t}}^{\mathrm{i\text{-}E}}$ illustrate that peak target power density between ELMs $\langle q_{\mathrm{max}} \rangle_{\mathrm{t}}^{\mathrm{i\text{-}E}}$ was steady around $\approx 1 \mathrm{MW} \cdot \mathrm{m}^{-2}$ in the unswept feedforward plasma, but very obviously oscillated in sympathy with OSP sweeping in the RTC one. In other words, the heat load too rose and fell with sweeping, tending to be lower for the OSP closest to the pumping duct. Moreover it formed a profile roughly twice as peaked on average in sample Pulse No's 79518 as in 76681 (viz. $A_{\mathrm{outb.\ tgt}} \langle q_{\mathrm{max}} \rangle_{\mathrm{t}}^{\mathrm{i\text{-}E}} / \langle P_{\mathrm{outb.\ tgt}} \rangle_{\mathrm{t}}^{\mathrm{i\text{-}E}}$, where $A_{\mathrm{outb.\ tgt}}$ is area of the outboard target). These changes in power profiles and ELM occurrence, described above, probably contributed to the large drop in $\langle P_{\mathrm{outb.\ tgt}} \rangle_{\mathrm{t}}^{\mathrm{i\text{-}E}} / \langle P_{\mathrm{in}} \rangle_{\mathrm{t}}$ seen first upon introduction of sweeping (orange diamonds labelled "0"), before RTC addition of nitrogen progressively decreased it further. Equivalence of inter-ELM average load with unswept feedforward or swept RTC seeding, despite often lower $\langle f_{\mathrm{rad}}^{\mathrm{tot}} \rangle_{\mathrm{t}}^{\mathrm{i\text{-}E}}$ for the latter, points to its power balance involving a greater proportion of exhaust in the ELMs and associated radiation themselves. This departure is exemplified by again a much smaller change in the fraction of input power deposited on $A_{\mathrm{outb.\ tgt}}$ averaged over the ten largest transients in each chosen 2 s window (top right pane Fig.3), i.e. ELMs were less strongly affected in the swept RTC series. Hence full reduction of target load when using RTC seeding would still rely upon some compatible form of active ELM control [21].

On the other hand, global plasma performance in terms of energy confinement factor [22] $\langle \mathrm{H}_{98\mathrm{y}} \rangle_{\mathrm{t}}$ itself varied less with swept RTC, such that for highest $\langle \mathrm{NVA} \rangle_{\mathrm{t}}^{\mathrm{i\text{-}E}}$ it stayed very close to unity (top pane Fig.4), noticeably better than under unswept feedforward seeding. Simultaneously, line-average density normalised to the Greenwald value [23] $\langle f_{\mathrm{Gwd}} \rangle_{\mathrm{t}}$ was kept near 90% in both schemes (middle pane Fig.4). Above all, however, line-average effective ionic charge $\langle Z_{\mathrm{eff}} \rangle_{\mathrm{t}}$ maintained a manifestly lower level in the swept RTC plasmas (bottom pane Fig.4), indicative of significantly improved bulk purity over unswept feedforward behaviour. These global contrasts, as well as that in ELM response, actually reflect the outcome that much less nitrogen was injected using swept RTC, its integrated input being only $\approx 40\%$ of that in unswept feedforward pulses at comparable highest $\langle \mathrm{NVA} \rangle_{\mathrm{t}}^{\mathrm{i\text{-}E}}$. Real-time control combined with OSP sweeping therefore allowed a more effective usage of the extrinsic species, with on average a greater net influence on target inter-ELM heat load per injected ion.

Preliminary tests of OSP sweeping plus RTC of nitrogen seeding via a VUV spectroscopic signal in high-triangularity Type I H-mode on JET have consequently demonstrated strong moderation of divertor power load between ELMs, as will be required in the forthcoming ILW upgrade with

enhanced NBI heating. Relative to previous unswept feedforward cases achieving similar low levels of inter-ELM exhaust, significantly less nitrogen was injected using both sweeping and RTC, causing less degradation of other plasma properties. Global energy confinement, for example, remained within a few percent of the ITERH98(y,2) scaling law [22] for line-average density close to 90% of the Greenwald value, while plasma purity measured by line-average $\langle Z_{\mathrm{eff}} \rangle_{\mathrm{t}}$ was unchanged from unswept unseeded reference cases at the same deuterium fuelling rate. For just $\approx 7\%$ of input power landing on the outboard target between ELMs, the product $\langle H_{98\mathrm{y}} \rangle_{\mathrm{t}} \langle f_{\mathrm{Gwd}} \rangle_{\mathrm{t}} / \langle Z_{\mathrm{eff}} \rangle_{\mathrm{t}}$ hus retained a figure of ≈ 0.49 exploiting swept RTC, versus ≈ 0.34 for unswept feedforward seeding. Feedback control should also particularly promote more stationary conditions as pulse flat-tops are gradually extended up to 20s in the upgraded JET. The major qualification remains transient effluxes in ELMs, which are similarly less affected under the OSP-swept, RTC-seeding scheme, and would require compatible active control for full abatement of the divertor load.

ACKNOWLEDGEMENTS

This work, part-funded by the European Communities under the contract of Association between EURATOM and CCFE, was carried out within the framework of the European Fusion Development Agreement. The views and opinions expressed herein do not necessarily reflect those of the European Commission. This work was also part-funded by the RCUK Energy Programme under grant EP/I501045.

REFERENCES

[1]. J. Pamela *et al*., Journal of Nuclear Materials, **363 - 365** (2007) 1
[2]. G.F. Matthews *et al*., Physica Scripta **T128** (2007) 137
[3]. P. Andrew *et al*., Journal of Nuclear Materials, **266 - 269** (1999) 153
[4]. P. Andrew *et al*., Nuclear Fusion, **47** (2007) 1112
[5]. T. Loarer *et al*., Journal of Nuclear Materials, **390 - 391** (2009) 20
[6]. P. Mertens *et al*., Journal of Nuclear Materials, **390 - 391** (2009) 967
[7]. V. Riccardo *eet al*., Physica Scripta **T138** (2009) 014033
[8]. D. Ćirić *et al*., Fusion Engineering Design, **82** (2007) 610
[9]. G.P. Maddison *et al*., "Moderation of target loads using fuelling and impurity seeding on JET" 19th Plasma-Surface Interactions Conference, San Diego, USA (May 2010) paper O-23, *accepted for* Journal of Nuclear Materials
[10]. G.P. Maddison *et al*., "Moderation of divertor heat loads by fuelling and impurity seeding in well-confined ELMy H-mode plasmas on JET", *submitted to* Nuclear Fusion
[11]. A.M. Messiaen *et al*., Nuclear Fusion, **34** (1994) 825
[12]. A. M. Messiaen *et al*., Physics Review Letters, **77** (1996) 2487
[13]. A. Kallenbach *et al*., Nuclear Fusion, **35** (1995) 1231
[14]. A. Kallenbach *et al*., Nuclear Fusion, **49** (2009) 045007
[15]. M.F.F. Nave *et al*., Nuclear Fusion, **43** (2003) 1204
[16]. G.R. Saibene *et al*., Plasma Physics and Controlled Fusion, **44** (2002) 1769
[17]. A. Loarte *et al*., Plasma Physics and Controlled Fusion, **44** (2002) 1815

[18]. T. Eich *et al*., "Power load studies in Type I ELMy H-modes in JET" 19th Plasma-Surface Interactions Conference, San Diego, USA (May 2010) paper O-06, *accepted for* Journal of Nuclear Materials
[19]. J. Van de Vegte., "Feedback Control Systems" (Prentice-Hall, New Jersey, 1990) p. 176
[20]. R. Felton *et al*., Fusion Engineering Design, **74** (2005) 561
[21]. E. de la Luna *et al*., APS Division of Plasma Physics 51st Annual Meeting, Atlanta, USA (Nov. 2009) http://meetings.aps.org/link/BAPS.2009.DPP.PI2.2
[22]. ITER Physics Basis Expert Groups on Confinement & Transport and Confinement Modelling & Database, ITER Physics Basis Editors, Nuclear Fusion, **39** (1999) 2175.
[23]. M. J. Greenwald *et al*., Nuclear Fusion, **28** (1988) 219.

	N_2 seeding		D_2 fuelling
	feedforward	feedback	feedforward
unswept	✓		✓
OSP sweeping (4 Hz)		✓	✓

Table 1. Specification of ELMy H-mode experiments referred to in the present report. Feedforward D_2 fuelling was applied throughout all cases. (Results from refs.[9,10] provide the feedforward comparison points (circles) in Figs.3 & 4 .)

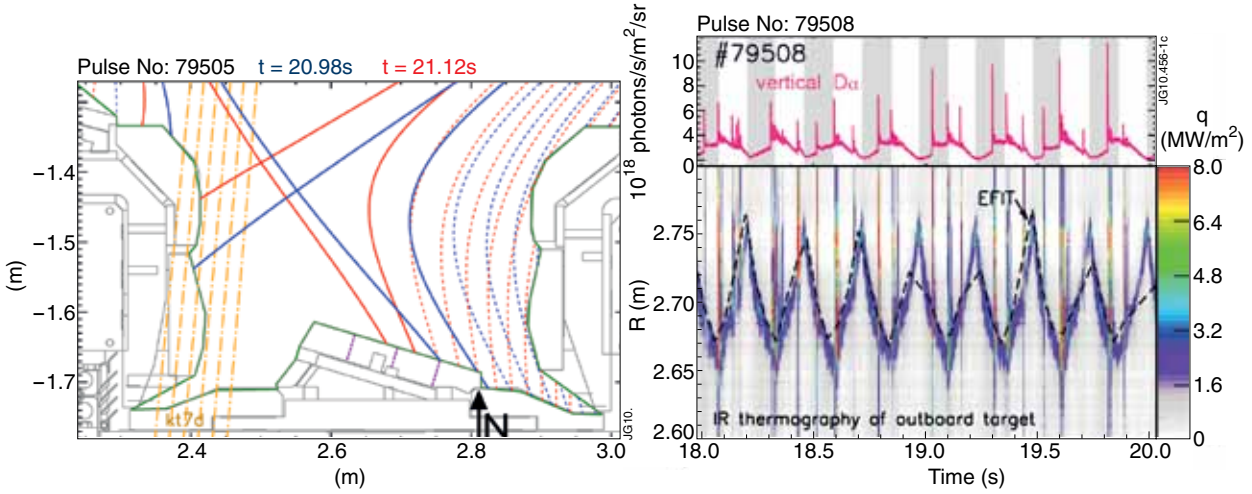

Figure 1: (a) EFIT magnetic reconstructions within the divertor close to times of the Outboard Strike-Point (OSP) extrema during sweeping. Scrape-off layer flux surfaces traced are separated by 1 cm at the outboard mid-plane. Also superimposed : (vertical arrow) location of nitrogen input during extrinsic seeding; (dot-dash lines labelled "kt7d") view of the VUV divertor spectrometer; (violet dotted lines) where the main outboard target tile will be divided into four thermally-separated, solid W stacks in the ITER-like wall (ILW) upgrade. (b) Actual motion of the OSP measured by fast infra-red thermography during triangular-waveform sweeping at 4Hz. Displacement of ≈ 10cm is visible. Superimposed : (black dashed line) OSP position calculated by EFIT ; (top) Da emission along a vertical line-of-sight outside the divertor. Phases of OSP moving inwards shaded, moving outwards clear.

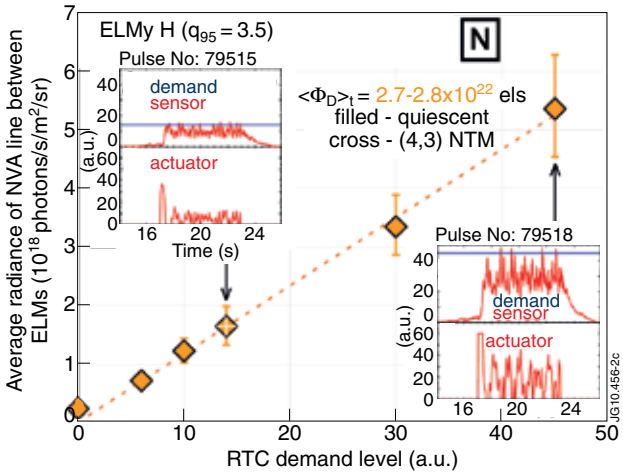

Figure 2: Response to demand level of Real-Time-Controlled (RTC) nitrogen seeding, in terms of average brightness of the NVA (20.93 nm) line between ELMs. Superimposed : (dotted line) exact direct proportionality. Insets : examples of RT network signals, showing demand level, filtered spectroscopic sensor (NVA), and resulting actuator output delivered to the nitrogen injection module (vertical scales in arbitrary units).

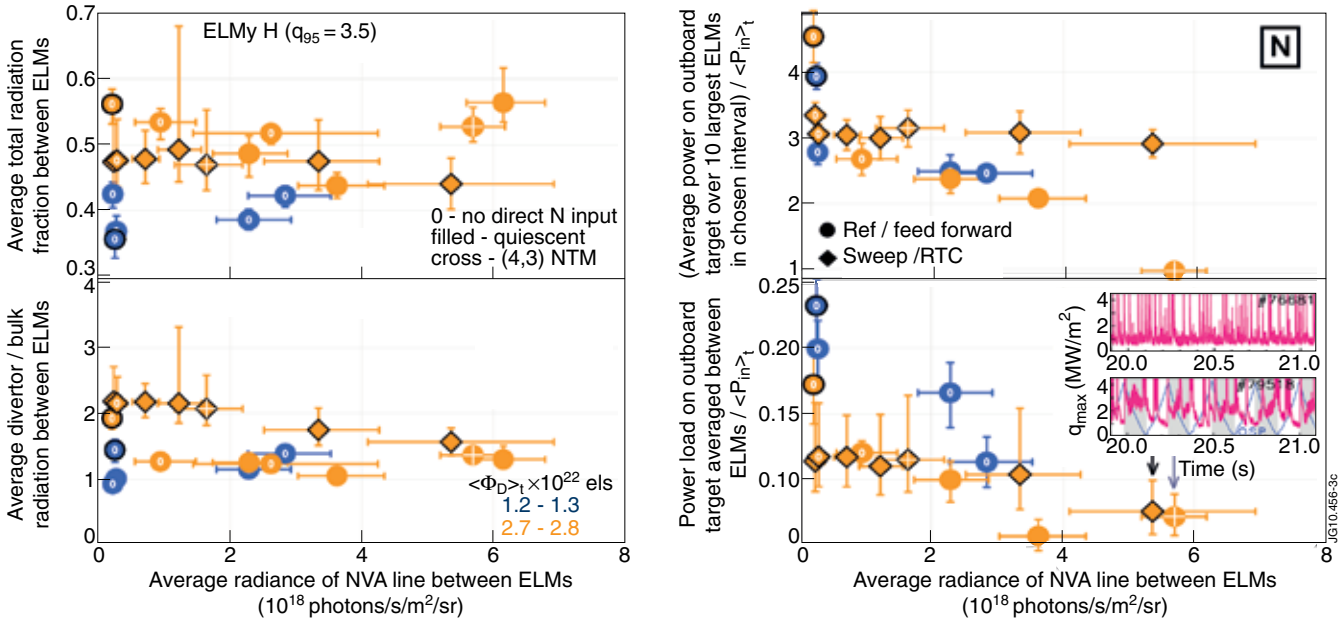

Figure 3: Comparison of series including OSP sweeping and RTC seeding (black-outlined circles & diamonds) with unswept feedforward counterparts (circles). Points colour-coded according to their D-fuelling level, those labelled "0" with no direct N input. Top left : total radiation fraction averaged between ELMs. Bottom left : average ratio of divertor to bulk radiation between ELMs. Top right : power landing on the whole outboard target averaged over the 10 largest ELMs in each chosen flat-top window, normalised by total input power. Three feedforward cases with an outward-shifted OSP omitted. Bottom right : average power landing on the outboard target between ELMs, normalised by total input power. Outward-shifted-OSP feedforward cases again excluded. Insets: traces of peak power density on the outboard target for respective plasmas with highest average inter-ELM NVA emission. OSP sweeping in the RTC pulse (Pulse No: 79518) also indicated, with phases of OSP moving inwards shaded, moving outwards clear.

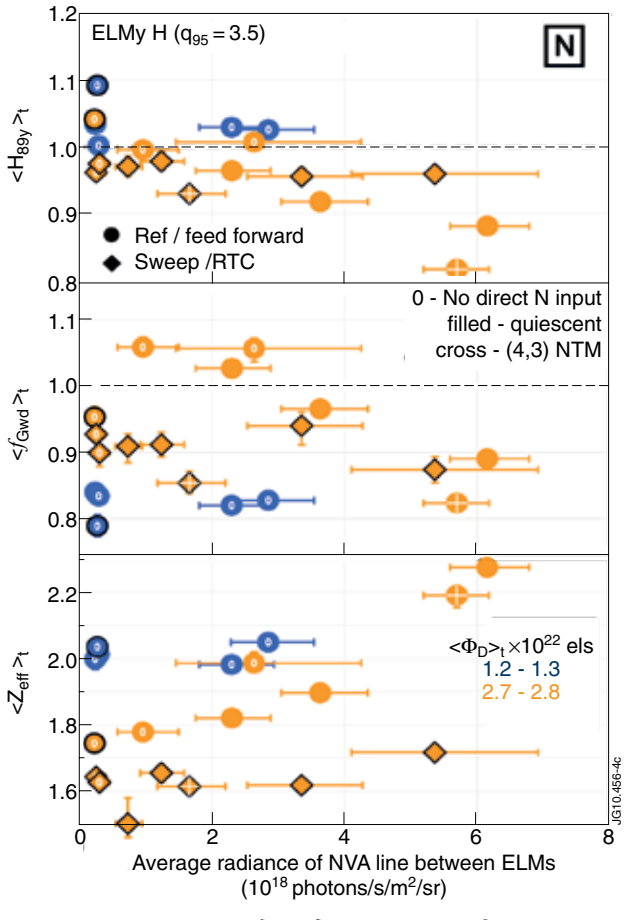

Figure 4: OSP-swept, RTC-seeded and unswept, feedforward-seeded plasmas, key as in Fig.3. Top : global energy confinement normalised to the ITERH98(y,2) scaling law [22]. Middle : central line-average electron density normalised to the Greenwald value [23]. Bottom : central line-average effective ionic charge, from visible bremsstrahlung emission. Each ordinate is averaged over the whole chosen flat-top 2s window, including ELMs.